

The Globular Cluster Migratory Origin of Nuclear Star Clusters

M. Arca-Sedda^{1,2}, R. Capuzzo-Dolcetta¹

¹*Sapienza-Università di Roma, P.le A. Moro 5, I-00165 Rome, Italy*

²*University of Tor Vergata, Via O. Raimondo 18, I-00173 Rome, Italy*

Released 2014 Xxxxx XX

ABSTRACT

Nuclear Star Clusters (NSCs) are often present in spiral galaxies as well as resolved Stellar Nuclei (SNi) in elliptical galaxies centers. Ever growing observational data indicate the existence of correlations between the properties of these very dense central star aggregates and those of host galaxies, which constitute a significant constraint for the validity of theoretical models of their origin and formation. In this paper we give statistical relevance to the well known ‘migratory and merger’ model for NSC and SN formation, obtaining a set of parameters to correlate with the host parameters. We find that the correlations between the masses of NSCs in the migratory model and the global properties of the hosts reproduce quite well the observed correlations, supporting the validity of the migratory-merger model.

Key words: galaxies: nuclei, galaxies: star clusters; methods: numerical.

1 INTRODUCTION

Due to the ever growing quantity of high resolution data, in the last few years great interest has been focused on the central region of galaxies where various phenomena co-exist.

Thanks to the high resolution images provided by the Hubble Space Telescope, it is clear, nowadays, that the nuclei of the majority of both elliptical and early type spiral galaxies ($M > 10^{10} M_{\odot}$) harbour massive or supermassive black holes (SMBHs), whose masses, M_{BH} , range in the $10^6 - 10^9 M_{\odot}$ interval and may be up to $\sim 10^{10} M_{\odot}$ as in the case of the SMBH in NGC1277 (van den Bosch et al. 2012). In some cases, the central SMBH is surrounded by a massive, very compact, star cluster commonly referred as Nuclear Star Cluster (NSC).

NSCs are observed in galaxies of every type of the Hubble sequence (Böker 2002; Côté et al. 2006) and their modes of formation and evolution are still under debate. In the case of elliptical galaxy hosts, the nuclear clusters are also referred to as ‘resolved stellar nuclei’. For the sake of this paper we will refer to NSCs or resolved stellar nuclei indifferently. NSCs are sited at the photometric and kinematic centre of the host galaxy, i.e. at the bottom of the potential well (Böker et al. 2002; Neumayer & Walcher 2012). This is likely connected to a peculiar formation history. As a matter of fact, all NSCs contain an old stellar population ($age > 1$ Gyr) and most of them show, also, the presence of a young population, with ages below 100 Myr (Rossa et al. 2006; Seth et al. 2010; Neumayer & Walcher 2012).

NSCs are bright (about 4 mag brighter than ordinary

globular clusters), massive objects ($10^6 - 10^7 M_{\odot}$), very dense and with a half-light radius of 2 – 5 pc. Their small sizes and large masses make them the densest stellar systems in the Universe (Neumayer 2012).

The relation between NSCs and SMBHs is poorly known; they seem to be two ‘faces of the same coin’, constituting central massive objects (CMOs) whose actual presence depends on the host mass: galaxies with mass above $10^{10} M_{\odot}$ usually host an SMBH while lighter galaxies have, instead, a well resolved central star cluster (an NSC). Moreover, a transition region exists for galaxies with mass between 10^8 and $10^{10} M_{\odot}$ in which both the objects co-exist (Böker et al. 2002; Böker 2010; Graham 2012).

With regard to the lack of evidence of NSCs in high mass ($> 10^{11} M_{\odot}$) galaxies, one possible explanation is the formation of giant ellipticals through merging of smaller galaxies (Merritt 2006). Quantitatively speaking, Bekki & Graham (2010) simulations showed that if the two colliding galaxies host MBHs, a black hole binary (BHB) could form which heats up the resulting stellar nucleus causing its progressive evaporation. This process can destroy the super cluster, shaping significantly the density profile of the merger product and leaving behind a BHB that shrinks due to gravitational wave emission leading eventually to a SMBH. Another possibility is that in the early phase of the galaxy life, an initial NSC could be the seed for the BH birth as suggested first by Capuzzo-Dolcetta (1993) and later by Neumayer & Walcher (2012) and Gnedin, Ostriker & Tremaine (2014).

Recently, a number of researchers studied the existence of scaling relations between NSCs and their galactic hosts; similar studies have already been done, seeking for scaling relations between SMBHs and their hosts. However, it is still unclear the robustness of the NSC-galaxy relations and whether these relations are linked to those between SMBHs and the hosts.

For instance, Ferrarese et al. (2006) showed that the NSC mass (M_{NSC}) vs galaxy velocity dispersion (σ) relation is roughly the same of that observed for SMBHs. On the other hand, more recent studies (Leigh, Böker & Knigge 2012; Graham 2012) claim that the $M_{\text{NSC}}-\sigma$ relation is shallower than for SMBHs, $M_{\text{NSC}} \propto \sigma^{1.5}$. Moreover, it has been shown that while SMBH masses correlate with the galaxy mass, the NSC masses correlate better with the bulge mass (Erwin & Gadotti 2012).

At present, two are the most credited frameworks for the NSC formation.

One scenario refers to the so called (dissipational) 'in-situ model' (King 2003, 2005; Milosavljević 2004; Bekki, Couch & Shioya 2006).

According to this model, an injection of gas in the central region of a galaxy hosting a 'seed' black hole could lead to the formation of a NSC if the typical crossing time of the parental galaxy is shorter than the so-called 'Salpeter time', which is the time-scale over which the central BH can grow by accretion (Nayakshin, Wilkinson & King 2009).

Another (dissipationless) scenario invokes the action of the dynamical friction process which makes massive globular clusters (GCs) sink toward the centre of the host galaxy (Tremaine, Ostriker & Spitzer Jr. 1975; Peisce, Capuzzo-Dolcetta & Vietri 1992; Capuzzo-Dolcetta 1993). Their subsequent merging leads to a super star cluster with characteristics indistinguishable from those of an NSC (Capuzzo-Dolcetta & Miocchi 2008b,a). This scenario is often referred to as infall-merger scenario or migratory-merger model.

Both the theories above encounter some troubles in explaining completely the NSC formation. According to some qualitative considerations, the in situ model would predict too massive NSCs, while a possible problem for the GCs infall model is that it would give lighter NSCs than observed (Leigh et al. 2012). Hartmann et al. (2011) say that mergers of star clusters are able to produce a wide variety of observed properties, including densities, structural scaling relations, shapes (including the presence of young discs) and even rapid rotation, nonetheless claim that some kinematical properties of observed NSCs are hardly compatible with merger models. They suggest the need of a 50% of gas in the overall scheme.

Turner et al. (2012) referring to their Fornax ACS survey and to some speculative considerations conclude that, for galaxies and nuclei in their sample, the infall formation mechanism is the more likely for low to intermediate mass galaxies while for more massive ones accretion triggered by mergers, accretions, and tidal torques is likely to dominate. The two mechanisms smoothly vanish their efficiency on the intermediate mass galactic range, and they indeed provide some evidence of "hybrid nuclei" which could be the result of parallelly acting formation mechanisms.

While the in-situ model has remained almost speculative and difficult to constrain to available observa-

tions, several authors provided detailed numerical tests for the GC merger scenario starting from the original idea in Capuzzo-Dolcetta (1993). The first simulations were done by (Capuzzo-Dolcetta & Miocchi 2008b) and (Capuzzo-Dolcetta & Miocchi 2008a) in galaxy models without massive black holes and stellar discs; (Bekki 2010) studied the role of stellar discs and Antonini et al. (2012) the role of a central galactic MBH.

In particular, Antonini et al. (2012) made a full N -body simulation of the decay and merging of 12 GCs in a Milky Way model accounting for the presence of the Sgr A* $4 \times 10^6 M_{\odot}$ central black hole, obtaining an NSC that has global properties fully consistent with those observed in the nucleus of our galaxy. One recent work by Perets & Mastrobuono-Battisti (2014) presents the same merger simulations performed in Antonini et al. (2012) with the inclusion of different stellar populations in the various infalling globular clusters, and shows that infalling clusters can produce thick flattened structures with varied orientations, possibly related to 'disky' structures that are observed in galactic nuclei and clusters (see Mastrobuono-Battisti & Perets (2013) for a discussion of the evolution of such discs).

On another side, Antonini (2013a), by mean of a semi-analytical model, made some comparisons among the expected result of a merger scenario for the NSC formation and some scaling laws.

The aim of this paper is to check in a more complete and extensive way the reliability of the infall-merger model for the NSC formation. To reach this aim we build 'theoretical' scaling laws connecting NSC properties with those of the galactic hosts in a synthetic modelization of the global evolution of a Globular Cluster System (GCS) in a galaxy, considering the dynamical friction and tidal disruption as evolutionary engines. These scaling laws are to be compared with those observationally obtained.

The paper is organized as follows: in Section 2 the role of dynamical friction is discussed as well as the way we modeled galaxies and their GCS; in the same section the sample of data used for the comparison with observation is presented; Section 3 presents two different theoretical modelizations of the NSC growth in galaxies; in Section 4 we provide a set of 'theoretical' scaling laws which connect NSCs with their hosts and compare them with the observed laws; in Section 5, instead, we take into account the effect of tidal disruption of GCs on the resulting NSC mass. Finally, Section 6 is devoted to a summary of the main results, providing some general remarks such to draw conclusions.

2 THE GLOBULAR CLUSTER INFALL SCENARIO

The formation of a compact nucleus in the centre of a galaxy through the orbital decay of globular clusters has been discussed, first, by Tremaine et al. (1975). Working on a model of the M31 galaxy, they demonstrated that the efficiency of the dynamical friction mechanism could provide an amount of matter sufficient to form a compact nucleus of $10^7 - 10^8 M_{\odot}$ in the centre of this galaxy. Capuzzo-Dolcetta (1993) turned out the importance of considering the tidal disruption of the clusters as a competitive process that tunes

the effect of dynamical friction. Before approaching in a deeper way the theme, we now give a relevant analytical support to the idea that a NSC can grow in the centre of a galaxy by mean of GC decay in the innermost region via dynamical friction braking.

2.1 A preliminary, relevant scaling result

A direct and easy way to obtain a scaling between the mass accumulated to the galactic centre and the background velocity dispersion is based on the assumption that the galaxy has the mass density of a singular isothermal sphere

$$\rho(r) = \frac{v_c^2}{4\pi G r^2}, \quad (1)$$

where G is the gravitational constant, r is the galactocentric distance and v_c is the circular velocity, constant with radius and related to the velocity dispersion, σ , by $v_c = \sqrt{2}\sigma$.

Approximating the motion of the test mass, M , as a decreasing energy sequence of circular motions, the evolution equation of the modulus of the orbital angular momentum per unit mass, $\mathbf{L} = \mathbf{r} \wedge \mathbf{v}$, is

$$\dot{L} = \dot{r}v_c = -r \frac{F_{df}}{M}, \quad (2)$$

where F_{df} is the absolute value of the dynamical friction force exerted by the galaxy on the test object, which, using the Chandrasekhar's formula in its local approximation, is given by

$$F_{df}(r) = \frac{4\pi G^2 \ln \Lambda \rho M^2}{v_c^2} f(X), \quad (3)$$

with

$$f(X) = \text{erf}(X) - \frac{2X}{\sqrt{\pi}}, \quad (4)$$

where $X \equiv v_c/(\sqrt{2}\sigma)$ ($X = 1$ for a singular isothermal sphere), $\text{erf}(X)$ is the usual error function and Λ is the Coulomb logarithm. The time evolution of the radius $r(t)$ of the nearly circular orbit of the test mass under the previous assumptions is thus governed by the differential equation

$$\dot{r} = -\frac{G \ln \Lambda f(1)}{\sqrt{2}\sigma} \frac{1}{r}, \quad (5)$$

where $f(1) \simeq 0.4276$, which, with the initial condition $r(0) = r_0$, is easily integrated to give

$$r(t)^2 = r_0^2 - \frac{0.6047G \ln \Lambda M}{\sigma} t \quad (6)$$

and leads to $T = \sigma r_0^2/(0.6047G \ln \Lambda M)$ as fully decay time ($r(T) = 0$). If the GC population follows the same isothermal distribution of galactic stars, their mass enclosed in a sphere of radius r is

$$M_{\text{GCS}}(r) = A \frac{2\sigma^2}{G} r, \quad (7)$$

where A is a normalization constant related by the expression $A = GM_{\text{GCS}}/(2\sigma^2 R)$ to the total GC mass, M_{GCS} , which is the sum of the masses of GCs contained in the edge of its initial distribution ($r \leq R$). If the GCs dynamically decayed to the galactic centre go to grow a nucleus therein, the value of the nucleus mass at any age t of the galaxy, $M_n(t)$, is simply

$$\begin{aligned} M_n(t) &= M_{\text{GCS}}(\bar{r}(t)) = \\ &= \frac{2\sigma^2}{G} \sqrt{\frac{0.6047G \ln \Lambda M t}{\sigma}} = \\ &= 1.5553A \sqrt{\frac{\ln \Lambda M}{G}} \sqrt{t} \sigma^{3/2}, \end{aligned} \quad (8)$$

where $\bar{r}(t) = \sqrt{0.6047G \ln \Lambda M t/\sigma}$ is the maximum radius of the GC circular orbit decayed to the centre within time t .

In the case that GCs follow a different radial profile respect to the galaxy stars with, for instance, a power law $\rho_{\text{GCS}}(r) = Br^\alpha$, with $\alpha \neq -2$, the generalization of Equation 8 is

$$M_n(t) = \frac{2^{\frac{\gamma+5}{2}} A}{GR^{\gamma+2}} \sqrt{0.6047G \ln \Lambda M t}^{\frac{\alpha+3}{2}} \sigma^{\frac{1-\alpha}{2}}, \quad (9)$$

which, obviously, reduces to Equation 8 for $\alpha = -2$. Equation 9 gives a dependence of the nuclear mass on σ with a slope between 1/2 and 2, corresponding, respectively, to the extreme cases of initially flat GC distribution ($\alpha = 0$) and the steep r^{-3} decay. The relevant result here is that the slope of the $M_n - \sigma$ relation in the regime of dynamical friction dominated infall process is expected to be relatively small.

2.2 The data sample

The aim of this work is to show that the dry merger scenario can reproduce the correlations of observed NSCs with their hosts in a wide range of galaxy masses. To reach this aim, we need three important ingredients: i) a robust data base to compare our results with real observations of NSCs and their hosts, ii) a reliable treatment of the dynamical friction and tidal disruption processes and iii) a detailed model for the host galaxies to reproduce the environment in which GCs evolve.

The data base for the purposes of this work has been extracted from three different papers. The first (Erwin & Gadotti (2012), hereafter EG12), combines data coming from different works covering galaxies of the Hubble types S0-Sm; on another side, Leigh et al. (2012) (hereafter LKB12) provide data for 51 early type galaxies in the Advanced Camera Virgo Cluster Survey (Côté et al. 2004); finally, we considered data given in Scott & Graham (2013) (hereafter SG13) which is a collection of data from earlier works.

At the end, we gathered a total sample of 112 galaxies covering a wide range of Hubble types which contains several structural parameters of each galaxy such as mass, effective radius, velocity dispersion, and of the NSC masses.

To evaluate reliably the dynamical friction braking of GCs in their host galaxies, we have to assume galactic density profiles. As first approximation, we modeled galaxies as

spherically symmetric distributions in the form of Dehnen's spheres whose density is:

$$\rho_\gamma(r) = \frac{\rho_{\gamma 0}}{(r/R_g)^\gamma (r/R_g + 1)^{4-\gamma}}, \quad (10)$$

where $\gamma \geq 0$ and $\rho_{\gamma 0}$ is linked by

$$\rho_{\gamma 0} = \frac{(3-\gamma)M_g}{4\pi R_g^3},$$

to the total mass of the galaxy, M_g and to its length scale, R_g .

Generally, galaxies fainter than $M_V \sim -20.5$ show steep luminosity profiles with slope > 0.5 ('power-law' galaxies), while brighter galaxies show less pronounced cusps ('core' galaxies) (Lauer & et al. 2007; Merritt 2006), at least out to (3 – 10 arcsecs) from the galactic centre. Consequently, for each galaxy mass M_g , the γ exponent is randomly chosen in the range 0 – 0.3 for $M_g < 10^{10} M_\odot$, and in the range 0.5 – 1 for $M_g > 10^{10} M_\odot$. On the other side, it is not clear how the galaxy masses correlate with the parameter γ in the range $0.3 < \gamma < 0.5$.

It is relevant noting that the validity of 'true' cuspidal density profile models to describe the matter distribution of galaxies has been questioned by many authors that claim that the core-Sérsic profiles are better suited to describe the innermost (3 to 10 arcsecs) regions of early type galaxies (Graham 2004; Dullo & Graham 2012). However, since we are interested in the study of the dynamics of stellar clusters out from such small regions, we consider the simple γ density profiles as appropriate for our purposes. This choice allows us to use the results on dynamical friction recently obtained for cuspy Dehnen's profile (Arca-Sedda & Capuzzo-Dolcetta 2014).

Dehnen's profiles have a central cusp, and it has been demonstrated that the in density cusps the classical Chandrasekhar dynamical friction formula fails (see for instance Capuzzo-Dolcetta & Vicari (2005); Just et al. (2011)). To overcome this problem, Arca-Sedda & Capuzzo-Dolcetta (2014) provided a formulation for the dynamical friction process which is valid in cuspy galaxies, giving a useful fitting expression for the dynamical friction timescale (Arca-Sedda & Capuzzo-Dolcetta (2014), Equation 21):

$$\tau_{df} = \tau_0(2-\gamma)(4.93 - 3.93e) \left(\frac{M}{M_g}\right)^{-0.67} \left(\frac{r}{R_g}\right)^{1.76}, \quad (11)$$

where e is the orbital eccentricity of the text object of mass M and τ_0 is a normalization factor whose value is given by:

$$\tau_0(\text{Myr}) = 0.3 \sqrt{\frac{R_g^3}{M_{g,11}}},$$

where R_g (in kpc) is the scale radius and $M_{g,11}$ the total mass of the γ model galaxy in unit of $10^{11} M_\odot$. Equation 11 gives the dynamical friction decay time for a GC of mass M initially moving on an orbit of eccentricity $0 \leq e \leq 1$ in a spherical galaxy of mass M_g and length scale R_g .

Since τ_{df} depends, other than on e , on M_g , R_g and γ , to a good estimate of the dynamical friction time reliable values

of these three parameters are needed. In other words, it is important providing reliable models of the parent galaxy to ensure that the environment where dynamical friction acts is well reproduced. The simplest way to produce such model environments is via linking the parameters needed to establish the theoretical model to the observable quantities. As example, the LKB12 data sample contains the mass, M_g , and effective radius, R_e , which is the radius containing half of the total light. This parameter is important because it can be connected with the scale radius of the theoretical γ model, R_g . However, the data sample contains a limited number of galaxies in the range $10^8 - 10^{10} M_\odot$ and does not provide data for heavier galaxies, hence only a small fraction of the total range of galaxy masses could be investigated and, moreover, not always both the M_g and R_e values are available. To overcome these limitations, we need to extend with some proper extrapolations to a range of galaxies covering a wider, $10^8 - 10^{12} M_\odot$, mass interval. To this aim, we used data in LKB12 to correlate the galaxy mass with the effective radius and found a good fitting formula linking these two quantities as:

$$R_e(\text{kpc}) = 1.78 M_{g,11}^{0.14}, \quad (12)$$

where M_g is in units of $10^{11} M_\odot$. Then, given the galaxy mass we can evaluate its own effective radius, which is an astrophysical observable, and, finally, we get the scale length R_g by mean of these two relations (Dehnen 1993):

$$R_e = 3R_h/4, \quad (13)$$

$$R_h = \frac{R_g}{[2^{1/(3-\gamma)} - 1]}. \quad (14)$$

the first one being valid in the range of γ considered in this paper.

Finally, the scale length R_g is related to γ and M_g by this relation

$$R_g(\text{kpc}) = 2.37 \left(2^{1/(3-\gamma)} - 1\right) M_{g,11}^{0.14}. \quad (15)$$

In our modelization, we chose γ randomly in the range $[0 - 0.3]$ for $M_g < 10^{10} M_\odot$ and $[0.5 - 1]$ for $M_g \geq 10^{10} M_\odot$, in agreement with observations which suggest flatter cores for massive galaxies.

In Figure 1 the above $R_e - M_g$ curve is drawn together with observed data taken from LKB12.

On the other hand, to give an estimate of the total radius of the galaxy we developed the following relation:

$$R(\text{kpc}) = 31.62 R_g M_{g,11}^{1/6}, \quad (16)$$

which allows us to obtain total radii for our galaxy models going from few kpc for dwarf galaxies to several kpc for giant ellipticals, and give us an estimate of the maximum distance from the galactic centre allowed as initial position for the clusters.

As example, for a galaxy mass $M = 10^{12} M_\odot$ we obtain a radius $R \simeq 65 \text{kpc}$, that is a reasonable value for such

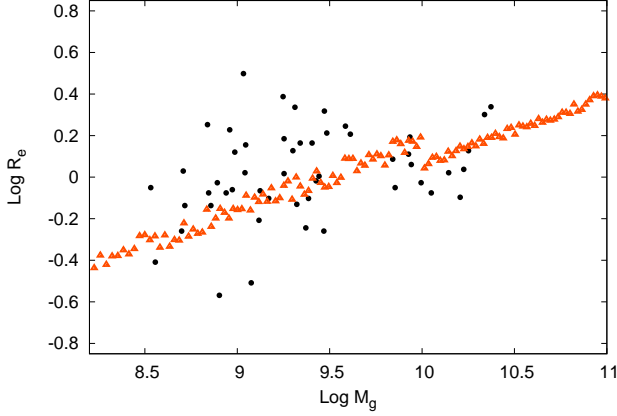


Figure 1. Effective radius as a function of the galaxy mass. Black filled circles are data given in LKB12 while the triangles represent the R_e estimated with Equation 13.

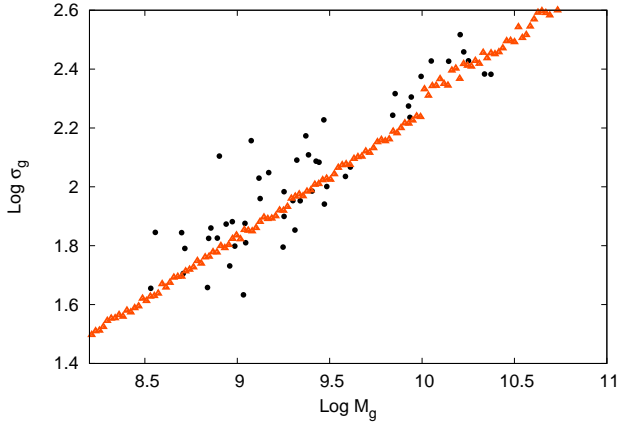


Figure 2. Modeled velocity dispersion (triangles) compared with observations (LKB12, filled circles).

galaxies (the supergiant elliptical galaxy M87 has a radius $R \leq 100\text{kpc}$, comparable to this value).

The other important parameter that we used to compare our galaxy models with real galaxies is the velocity dispersion, σ_g .

Following LKB12, to evaluate σ_g we used the formula given in Cappellari et al. (2006):

$$\sigma_g^2 = \frac{GM_g}{5f_\Omega R_g}, \quad (17)$$

where $f_\Omega = \Omega_b/\Omega_m$ is the baryonic mass fraction assumed $f_\Omega = 0.16$ as in LKB12.

Again, for any given galaxy mass, we selected randomly the parameter γ in the ranges explained above. The comparison between σ_g vs M_g in LKB12 with our estimate is shown in Figure 2.

Figures 1 and 2 convince us that we modeled the hosts sufficiently well to obtain reliable estimation of df times and, as a consequence, reliable values of the NSC masses.

Several authors had pointed out that the correlation between the bulge and the NSC mass is more dispersed than the $M_{\text{NSC}} - M_g$ relation (Erwin & Gadotti 2012). This is

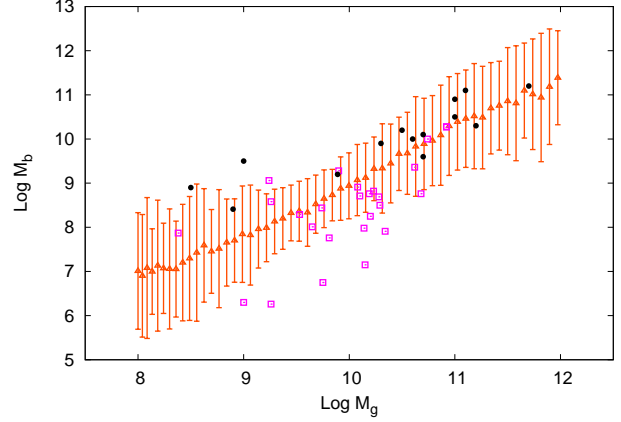


Figure 3. Bulge mass in our models (triangles) compared with observed values given in EG12 (squares) and SG13 (filled circles).

also related to the fact that many galaxies are actually bulgeless systems. Since it is very difficult to define a bulge in ellipticals, we evaluate it in our models by using the correlation bulge-host given in EG12:

$$\text{Log} \left(\frac{M_b}{10^{9.7} M_\odot} \right) = (1.23 \pm 0.17) \text{Log} \left(\frac{M_g}{10^{9.7} M_\odot} \right) + (-1.21 \pm 0.13). \quad (18)$$

This allows us to sample bulges in good agreement with the observed values, as it is shown in Figure 3.

Another fundamental ingredient in this framework is the globular cluster system (GCS) total mass.

A lower limit for the GCS mass could be obtained considering that the ratio between the NSC mass and the galaxy mass goes from $\sim 10^{-3}$ for small galaxies ($M_g \simeq 10^8 M_\odot$), up to 10^{-2} for the largest (M_g up to $10^{12} M_\odot$). This suggests a weak correlation between the GCS initial mass and the galaxy mass (Harris, Poole & Harris 2014).

We chose as expression for this correlation:

$$\frac{M_{\text{GCS}}(0)}{M_g} = 6.3 \times 10^{-3} M_{g,11}^{1/6}. \quad (19)$$

Due to that smallest galaxies host light globulars ($5 \times 10^3 - 5 \times 10^5 M_\odot$), while in heavier galaxies the globulars masses range in the $10^5 - 2 \times 10^6 M_\odot$ interval (Ashman & Zepf 1998), we set the minimum and maximum value of the GC mass as a function of the galaxy mass:

$$M_l = 5 \times 10^3 M_\odot (4 + \log M_{g,11}), \quad (20)$$

$$M_u = 5 \times 10^5 M_\odot (4 + \log M_{g,11}). \quad (21)$$

As we will show in Section 3.3, this choice gives mean GC masses in good agreement with observations.

3 THE MERGER SCENARIO

3.1 Analytical approach

A sufficiently accurate estimate of the NSC mass accumulated to the centre of the galaxy in the merger scenario may be given by means of the following considerations. Letting

$\Psi(M, r)dM d^3 \mathbf{r}$ be the (infinitesimal) number of GCs with mass in the $[M, M + dM]$ range and in the volume $d^3 \mathbf{r}$ centered at \mathbf{r} , the total mass of the GCS is:

$$M_{\text{GCS}} = \int_V \int_{M_l}^{M_u} M \Psi(M, r) dM d^3 \mathbf{r}, \quad (22)$$

where M_l and M_u indicate, respectively, the lower and upper value for the GC mass and V is the volume occupied by all the GCs. Keeping a sufficient level of generality, we can assume $\Psi(M, r)$ in the form of the product of a function of M and a function of r :

$$\Psi(M, r) = \Gamma_0 \xi(M) \chi(r), \quad (23)$$

where Γ_0 is a normalization constant given by

$$\Gamma_0 = \begin{cases} \frac{(2-s)M_{\text{GCS}}}{M_u^{2-s} - M_l^{2-s}} \frac{1}{N} & s \neq 2, \\ \frac{M_{\text{GCS}}}{\ln(M_u/M_l)} \frac{1}{N} & s = 2, \end{cases} \quad (24)$$

with $N = \int_0^R \chi(r) d^3 \mathbf{r}$ the total number of clusters in the galaxy.

A suitable expression for the mass function, $\xi(M)$, is a (truncated) power-law (see for instance Baumgardt (1998)):

$$\xi(M) = M^{-s}. \quad (25)$$

On the other hand, the distribution of radial positions is, in principle, arbitrary.

The simple inversion of Equation 11 yields the maximum radius, r_{max} , which contains all the clusters with mass $\geq M$ and with initial eccentricity $\leq e$ that have been confined around the galactic centre in a time $\leq t$:

$$r_{\text{max}} = R_g \left(\frac{t}{A_\gamma} \right)^{0.57} \left(\frac{M}{M_g} \right)^{0.38}, \quad (26)$$

with $A_\gamma = \tau_0(2 - \gamma)(1 + g(e))$.

Consequently, an estimate of the NSC mass as a result of the accumulation of GCs to the galactic centre, caused by dynamical friction, is:

$$M_{\text{NSC}}(t) = \Gamma_0 \int_{M_l}^{M_u} M^{1-s} N(r_{\text{max}}) dM, \quad (27)$$

with $N(r_{\text{max}})$ given by:

$$N(r_{\text{max}}) = 4\pi \int_0^{r_{\text{max}}} \chi(r) r^2 dr. \quad (28)$$

Let us now consider two different radial distributions for the GC population: a generic power-law distribution, $\chi(r) = Kr^\omega$, and a γ model density law (Equation 10).

In the first case, Equation 28 reduces to:

$$N(r) = \begin{cases} N \left(\frac{r}{R} \right)^{\delta+3} & r \leq R, \\ N & r > R, \end{cases} \quad (29)$$

with N the total number of clusters in the galaxy.

By substitution of this relation into Equation 27 we obtain:

$$M_{\text{NSC}}(t) = \Gamma C^n \int_{M_l}^{M_u} M^{1-s+0.38n} dM, \quad (30)$$

with $\Gamma = \Gamma_0 N$.

where $n = \omega + 3$ and C is a function of M_g, R_g, γ, e and t whose explicit expression is:

$$C = (t/A_\gamma)^{0.57} (1/M_g)^{0.38} R_g.$$

After integration, Equation 30 yields

$$M_{\text{NSC}}(t) = \Gamma C^n \frac{M_u^{2-s+0.38n} - M_l^{2-s+0.38n}}{2-s+0.38n}. \quad (31)$$

Looking at Equation 31, it is evident now the dependence of the NSC mass from the n parameter, i.e. from the steepness of the density profile.

The more general case in which we consider a γ density law, instead, will be discussed in the Appendix A.

3.2 Results of the analytical approach

Allowing δ to vary in Equation 31 we estimate the mass of the NSCs for different values of the slope of the GCs mass function s at varying the galaxy mass in the range $[10^8 - 10^{12}] M_\odot$.

Equation 31 allows us to see how the NSC mass increase as a function of time.

Figure 4 shows the NSC growth as a function of time in the case $\delta = 0$ for two extreme values of the galaxy mass (10^8 and $10^{12} M_\odot$) and three values of s considering the mass function in Equation 25, i.e. $s = (0, 2, 4)$ with M_l and M_u as defined by Equation 21.

The figure shows that the NSC mass increases rapidly in an early phase ($t \leq 1$ Gyr) to slow down later its growth. The slower increase in the case of larger values of s depends on the smaller fraction of heavy, and fast decaying, GCs for steeper mass functions.

Using the case $s = 2, \delta = 0$ as reference, we show in Figure 5 and 5 the ratio between the NSC mass evaluated letting $\delta = -1, -2$ and that obtained with $\delta = 0$ at fixed s and M_g .

Considering the case $M_g = 10^8 M_\odot$, it is evident that in an early phase ($t < 10^8 \text{ yr}$) the smaller δ the faster the NSC mass growth; however as the time increase is evident that the final mass of the cluster is slightly small with respect to the reference case $\delta = 0$ if $s = 0, 2$, while considering $s = 4$ the smaller the δ the greater the final mass of the NSC.

Considering instead more massive galaxies ($M_g = 10^{12} M_\odot$) we found that the smaller the δ the greater the final NSC mass.

Figure 7 shows the Mass of NSCs as a function of the host mass for $\delta = 0, -1, -2$ and $s = 0, 2, 4$. At any fixed value of s , there is not a significant difference between NSC masses estimate with different values of δ .

In Figure 8 we compare the theoretical NSC mass (that evaluated at $t = 13$ Gyr) with the observational values from EG12 and LBK12. The best agreement is achieved choosing $s = 2, \delta = 0$, as it will be more deeply discussed in Section 4. Moreover, we found that a good correlation is achieved in the case $s = 4, \delta = -2$, as it is shown in Figure 9, but this extreme case in which both the density profile and the mass function are very steep, is really unlikely to reproduce real

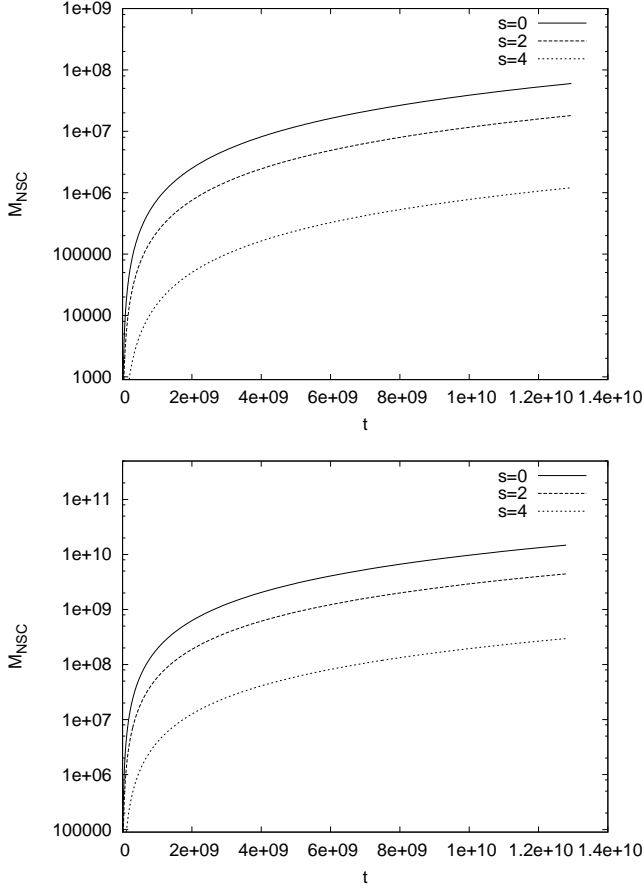


Figure 4. NSC mass growth for a galaxy with $M_g = 10^8 M_\odot$ (upper panel), and $M_g = 10^{12} M_\odot$ (bottom panel).

galaxies. For this reason, we limited the analysis to the case $s = 2, \delta = 0$. In the following, we refer to the model $s = 2$ as the combination ($s = 2, \delta = 0$).

In this context, it is relevant noting that the mass distribution of young luminous clusters (often referred to as YLCs) in many galaxies is a power-law with a spectral index ranging between $s = 1.8$ and $s = 2$ (Whitmore et al. 2010). Assuming such power-law as initial mass function for a GCS, Baumgardt (1998) showed that the evolution of such a system in a model of our galaxy, leads to a final mass function for the GCs in agreement with the actual mass function of the Milky Way GCS, giving us some confirmation about the choices made to model GCSs.

3.3 Statistical approach

Beside the 'analytical' method illustrated above to estimate the NSCs masses, we investigate the infall scenario also from a 'statistical' point of view, in order to obtain information on the radial distribution of GCs in the host galaxy, the number of globulars centrally decayed and that of GC survivors.

The idea behind this statistical approach is sampling the initial GCS of a given galaxy, and evaluate how many GCs sink toward the galactic centre within a Hubble time. A statistical estimate of the expected NSC mass is thus obtained by making N_s realizations of the GCS of a galaxy, in order to give constraints to the error. Each galaxy was

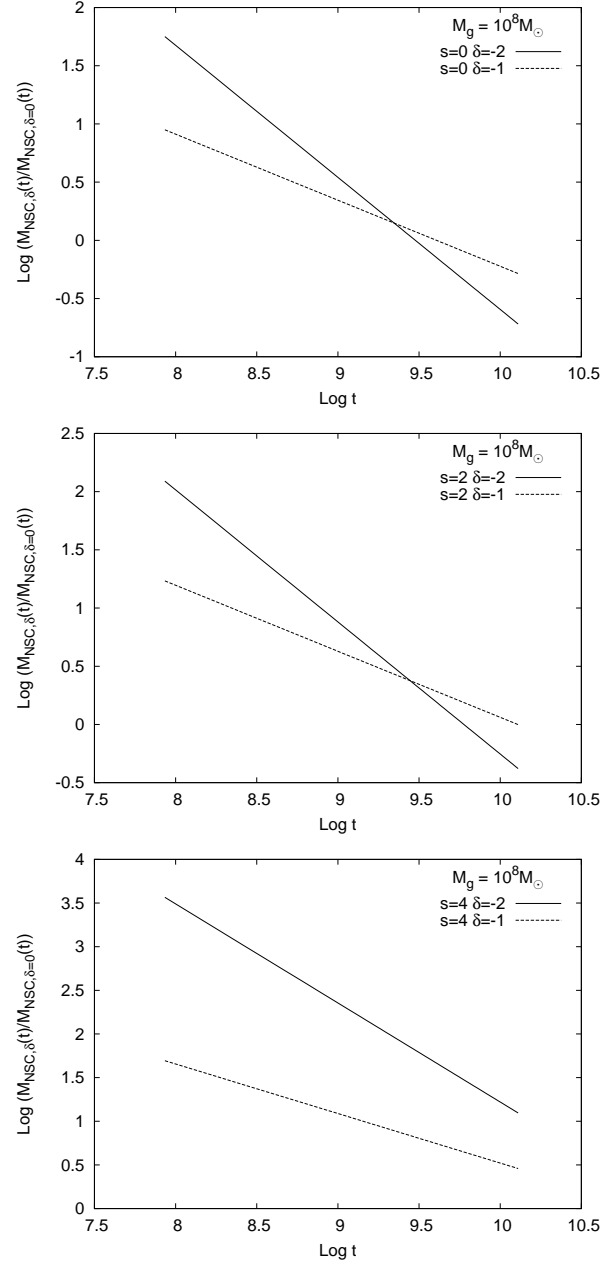


Figure 5. The ratio between the mass of NSC for a galaxy whose mass is $M_g = 10^8 M_\odot$ evaluate with $\delta = -2$ (straight line) and $\delta = -1$ (dotted line) and M_{NSC} obtained letting $\delta = 0$. From top to bottom, we set $s = 0, 2, 4$.

modeled as explained in Section 2.2, while, for each cluster, we sampled its initial radial position, r_0 , and orbital eccentricity, e , from a random, flat distribution.

From this GCS sampling we infer two relevant parameters to compare with observations. The first is the mean value of the GC mass for any given host mass, that can be compared with data given in LKB12; the second parameter is the number of survived clusters, which goes from few (< 10) GCs for small galaxies ($M_g \sim 10^8 M_\odot$), to few hundreds in intermediate mass galaxies, and up to 10^4 in giant ellipticals.

The relatively strong dependence of the df braking time

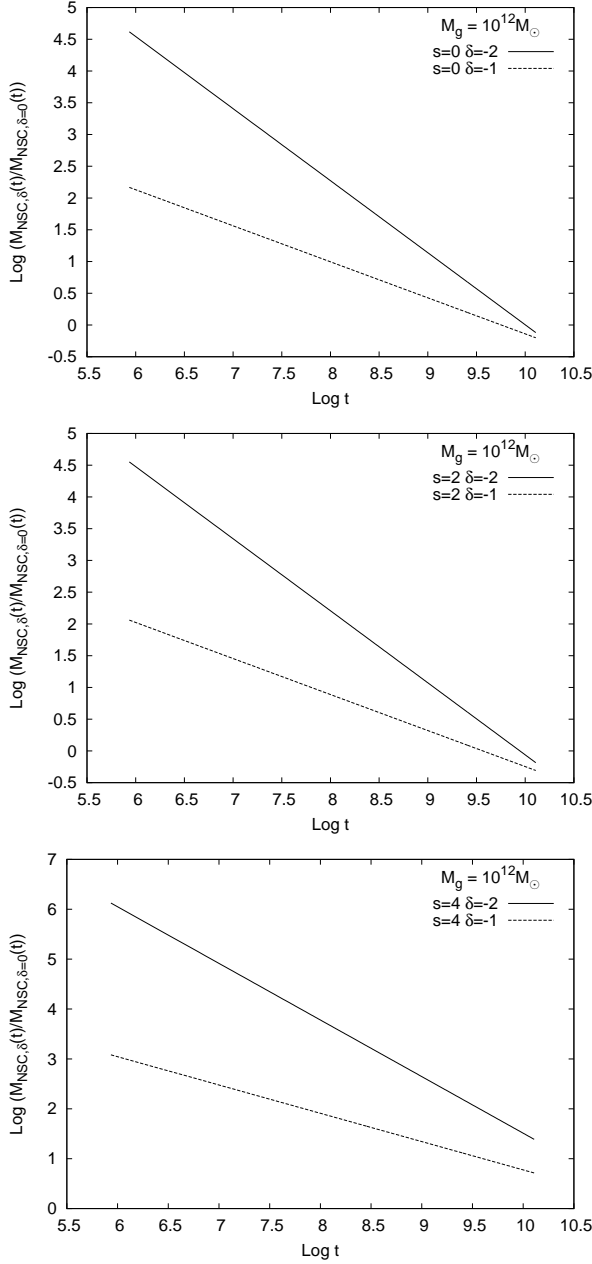


Figure 6. The same as in Figure 5, but for a galaxy with $M_g = 10^{12} M_\odot$.

on the individual GC mass (see Equation 11) deserves a careful treatment in the GC sampling, as explained in detail here below.

3.4 The statistical GCS modelization

As mentioned above, in this section we give estimate of the expected NSC mass for a given galaxy mass, sampling the whole GCS of the galaxy and looking at which clusters can sink toward the galactic centre within a Hubble time. Since initial position, eccentricity of the orbits and mass of each cluster are fundamental parameters in the evaluation of the decay time (see Equation 11), we vary the sampling method

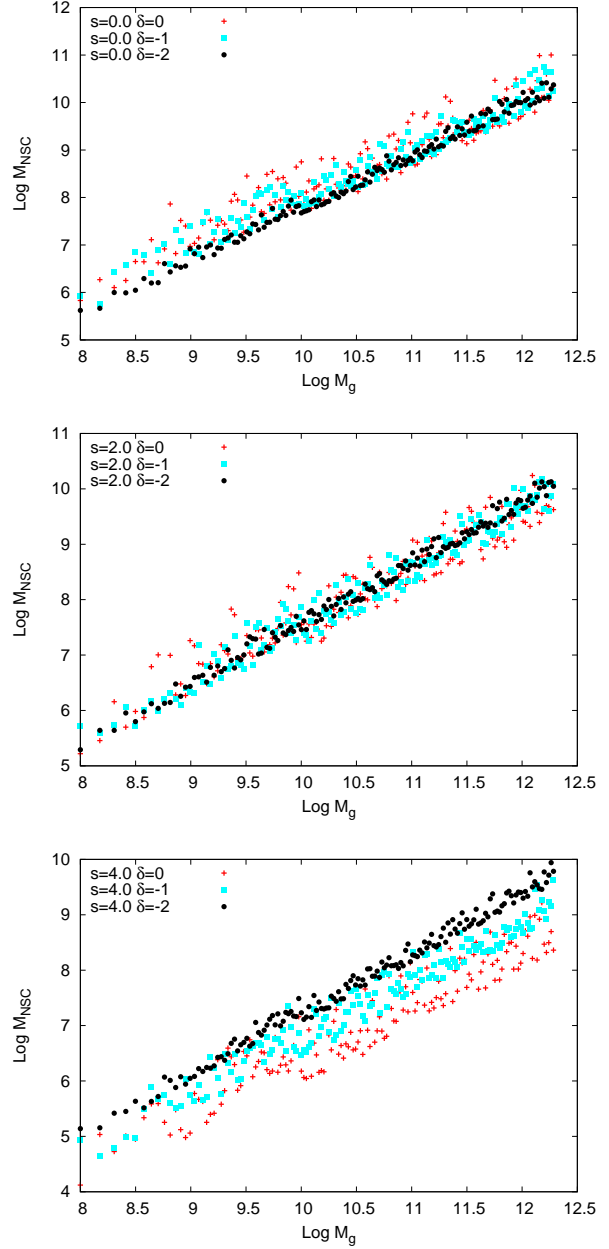


Figure 7. Masses of NSCs as a function of the host mass for different values of s and δ . From top to bottom, we set $s = 0, 2, 4$. In each panel, are shown results for $\delta = 0, -1, -2$.

for the GCS, changing spatial distribution and mass function of the clusters as explained in the following.

Flat radial density and mass power-law sampling (PLS)

This model (referred to as PLS model) is characterized by a flat spatial distribution of GCs within the radial range $[0 - R]$, with R the maximum distance defined in Equation 16; their eccentricities are sampled randomly between 0 and 1. GC masses are distributed according to a power-law distribution, $dN \propto M^{-s} dM$. PLS is, actually, the 'statistical version' of the analytical treatment (see Section 3.1). When

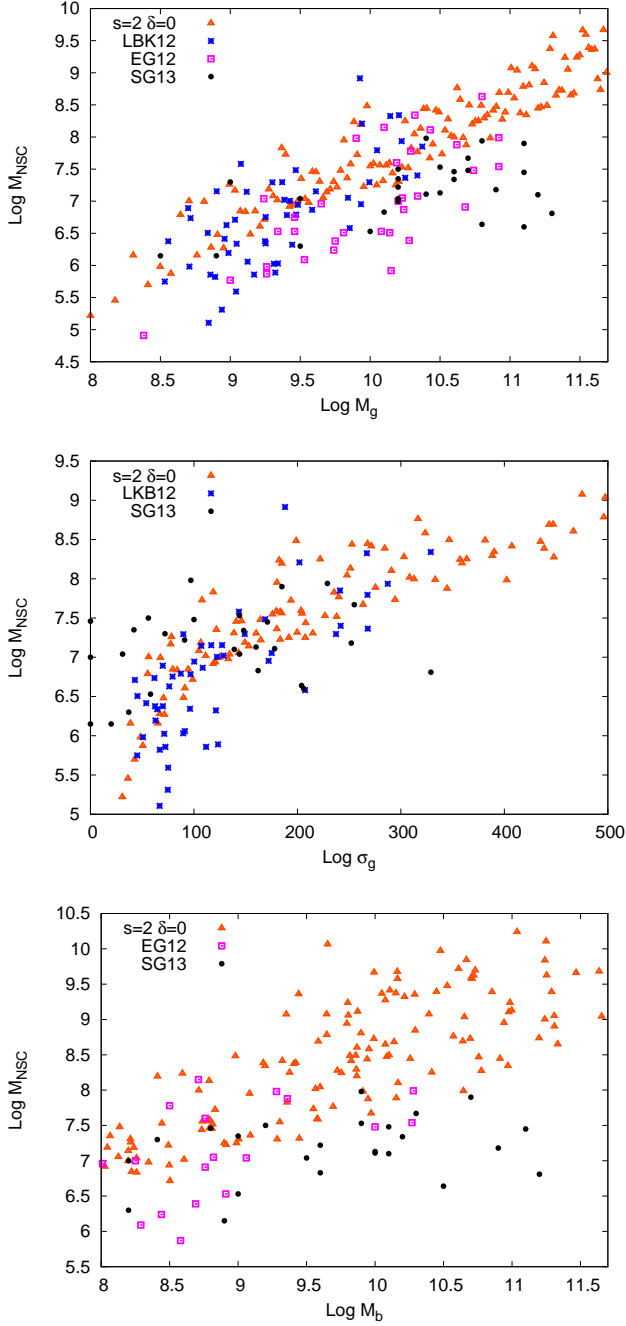


Figure 8. Theoretical NSCs masses vs. the host properties (triangles) estimated by using Equation 31 with $s = 2$, $\delta = 0$; compared with NSC masses from data in LKB12 (stars), EG12 (squares) and SG13 (filled circles). From top to bottom, the various panels give the correlation with hosts masses, velocity dispersion and bulge mass.

$s = 0$ (flat mass distribution) we refer to as the random sampling model, called RND.

Flat radial density and mass Gaussian sampling (GSS)

In the GSS model, the spatial location of GCs is the same as above, while the mass sampling is made by means of

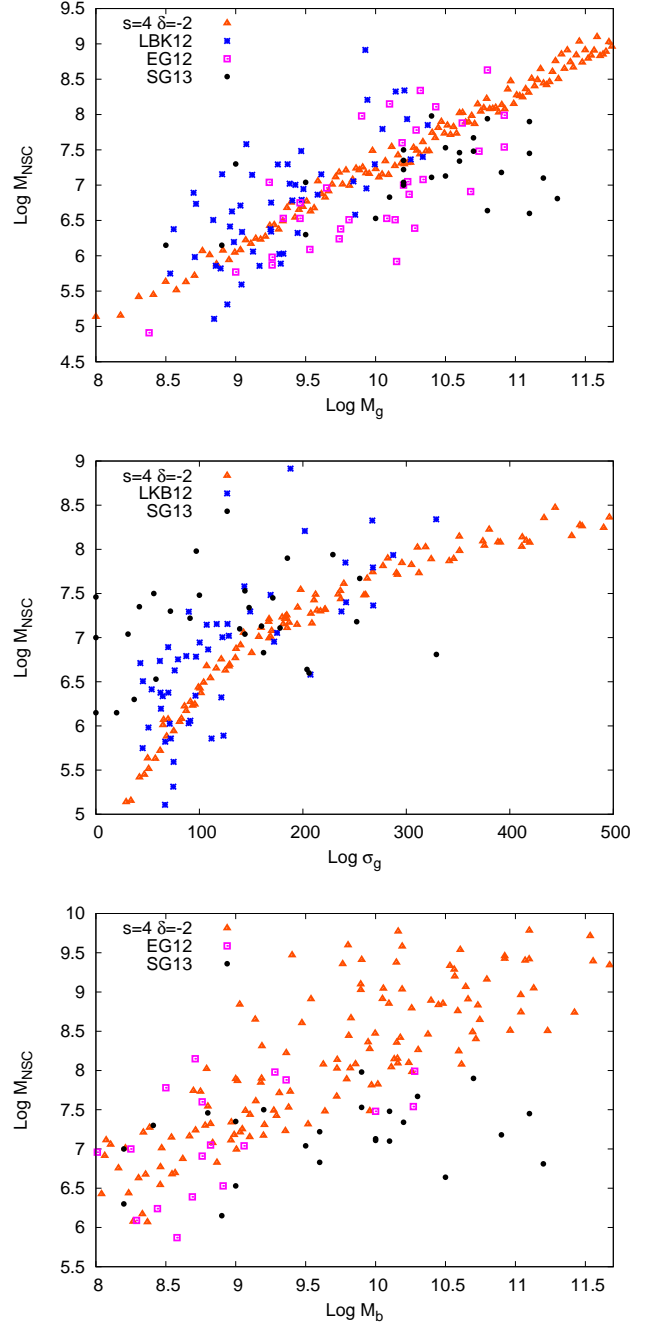


Figure 9. The same as in Figure 8, but in the case $s = 4$, $\delta = -2$.

a gaussian generator, given a mean value $M_{\text{mean}}/M_{\odot} = 10^5 [4 + \text{Log } M_{g,11}]$, and a fixed dispersion, $\sigma = 0.25$.

To exclude unrealistic, too light or too massive objects in the mass distribution, we truncated the gaussian at a low mass $M_l = 5 \times 10^3 M_{\odot}$ and at a high mass $M_u = 2 \times 10^6 M_{\odot}$.

ρ_r radial density sampling (RHO).

There is no compelling evidence that the GCs and stars of the parent galaxy followed, initially, different density profiles, so we found worth examining the case where the initial

GCS density profile is the same γ - profile of the parent galaxy.

3.5 Results of the statistical approach

The quality of our GC sampling can be tested by a comparison of the GCs mean masses obtained, M_{GC} , with data given in LKB12.

Looking at Figures 10, we see that GSS and RHO models give a decent agreement with observations in the whole range of masses covered by the data available; on the other hand, the RND model seems to overestimate the mean GC mass, while the PLS model gives an underestimate for host masses above $2 \times 10^9 M_\odot$.

Another relevant quantity obtainable with this approach is the number of ‘survived’ clusters, which can be compared with the actually observed clusters. In Figure 11 the fraction of decayed clusters as a function of the hosting galaxy mass is shown. Moreover, Figure 12 shows also the number of decayed clusters.

It should not surprise that for sufficiently massive galaxies ($M_g > 10^{10} M_\odot$) the number of survived GCs can exceed 10^4 . Many massive galaxies actually host such large populations of clusters. As example, the giant elliptical galaxy M87 (also known as Virgo A, with a mass $\sim 2 \times 10^{12} M_\odot$ (McLaughlin, Harris & Hanes 1994) hosts about 13,000 clusters, in agreement with our prediction.

Figures 13 show the ratio between the df decay time and the Hubble time for GCs belonging to a galaxy of mass $M_g = 10^{10} M_\odot$ whose GCS is sampled with the PLS, RND, GSS and RHO models. All clusters with $t_{df}/t_H < 1$ are decayed, therefore, the expected NSC mass is evaluated by summing the masses of all the decayed clusters, and in Figure 14 the resulting NSC mass vs. the host mass is reported.

However, it is not easy to understand which model fits better the observations. A more quantitative analysis is needed to reveal the real agreement, as, for instance, that of drawing scaling laws which connect the NSC mass with some of the host properties

In the following Section, we deepen the study of the comparison of our ‘theoretical’ and observed NSC, drawing the ‘theoretical’ scaling laws mentioned above to compare them with those actually observed. and actually observed scaling laws.

4 SCALING LAWS

As we said in the Introduction, the existence of correlations and scaling relations between the central compact object and the galactic host parameters may be an important clue to the understanding of the actual mechanisms of CMO formation.

It is well known that SMBH masses show a tight correlation with the host galaxy bulge velocity dispersion, σ_g , (Ferrarese et al. 2006) and with the galactic bulge mass, M_b , (see for example Marconi & Hunt (2003) and Häring & Rix (2004)). The implication claimed is that similar processes drove both SMBH and galaxy growth. In particular, Silk & Rees (1998) suggested that a feedback exists between the early stage of life of a galaxy and its central BH.

In the last years, many studies were devoted to derive,

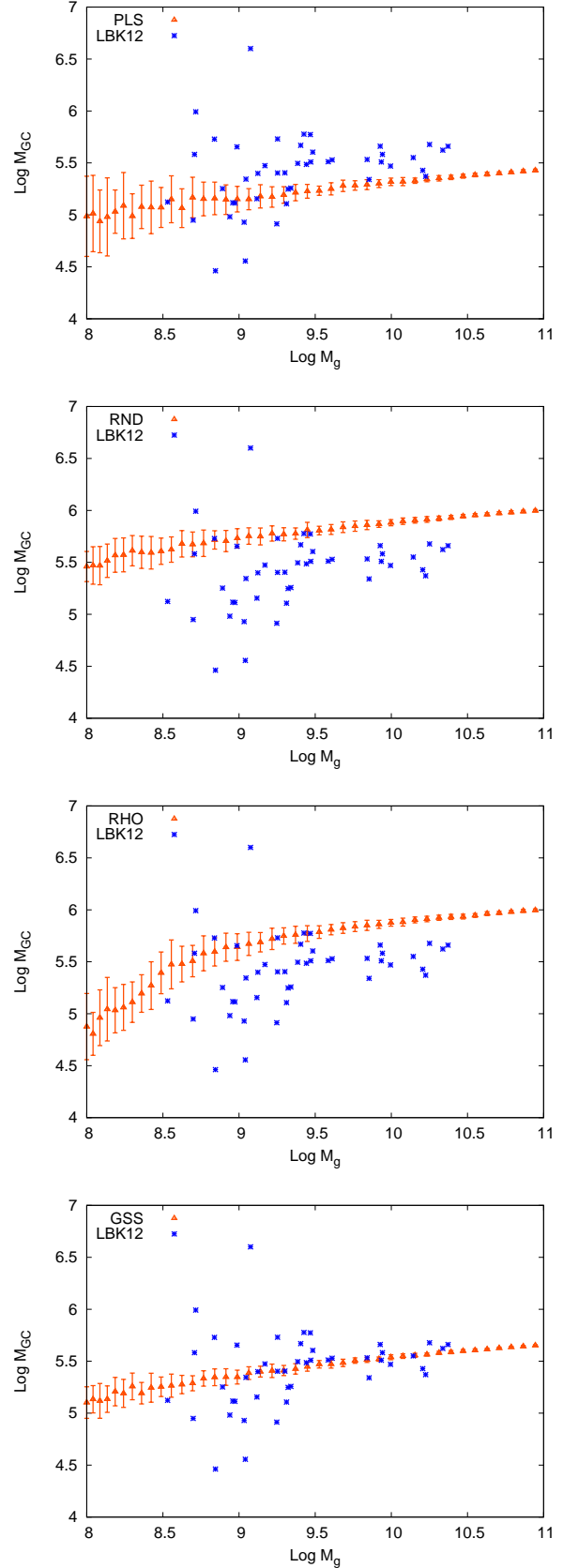


Figure 10. From top to bottom, mean GC mass in models PLS, RND, RHO and GSS as a function of the galaxy mass. Triangles represent our theoretical data while crosses represent the observations.

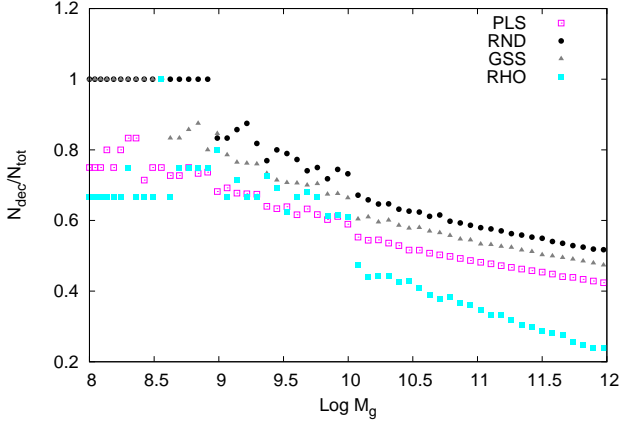


Figure 11. Number of decayed clusters over the total number of clusters within a Hubble time as a function of the host mass for each model considered.

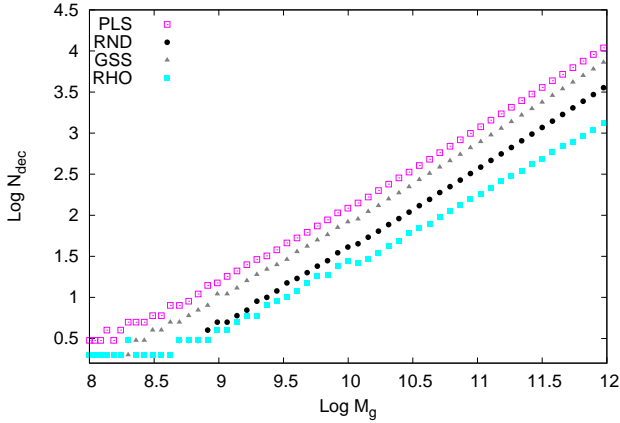


Figure 12. Number of decayed clusters within a Hubble time as a function of the host mass for each model considered.

also, scaling relations among NSCs and their host galaxies, finding that they follow relations in part similar as SMBHs do (Rossa et al. 2006). However, it is still unclear what, if any, the two different types of CMOs have in common, so to imply an intimate link between central galactic BHs and NSCs growth and evolution. Actually, differences in scaling relations of BHs respect to NSCs are being presently debated. As an example, Ferrarese et al. (2006) claimed that NSCs follow the same mass-sigma relation of massive central BHs, which is a power law with an exponent between 4 and 5. On the other side, Graham (2012) and Leigh et al. (2012) find a significantly shallower relation for the mass- σ relation of NSCs, with the exponent in the range 1.52 to 3.

At this regard, while the ‘in situ’ model is compatible with the steeper relation found in Ferrarese et al. (2006) (see for example McLaughlin, King & Nayakshin (2006)), the ‘dry merger’ scenario, instead, fits well with the Graham (2012) and Leigh et al. (2012) relations, as we have seen in Section 2.1 of this work (see also Antonini (2013b)).

By means of both the statistical and the analytical approaches presented above we can draw various correlations, including $M_{\text{NSC}} - M_g$ as well as $M_{\text{NSC}} - M_b$ and $M_{\text{NSC}} - \sigma_g$

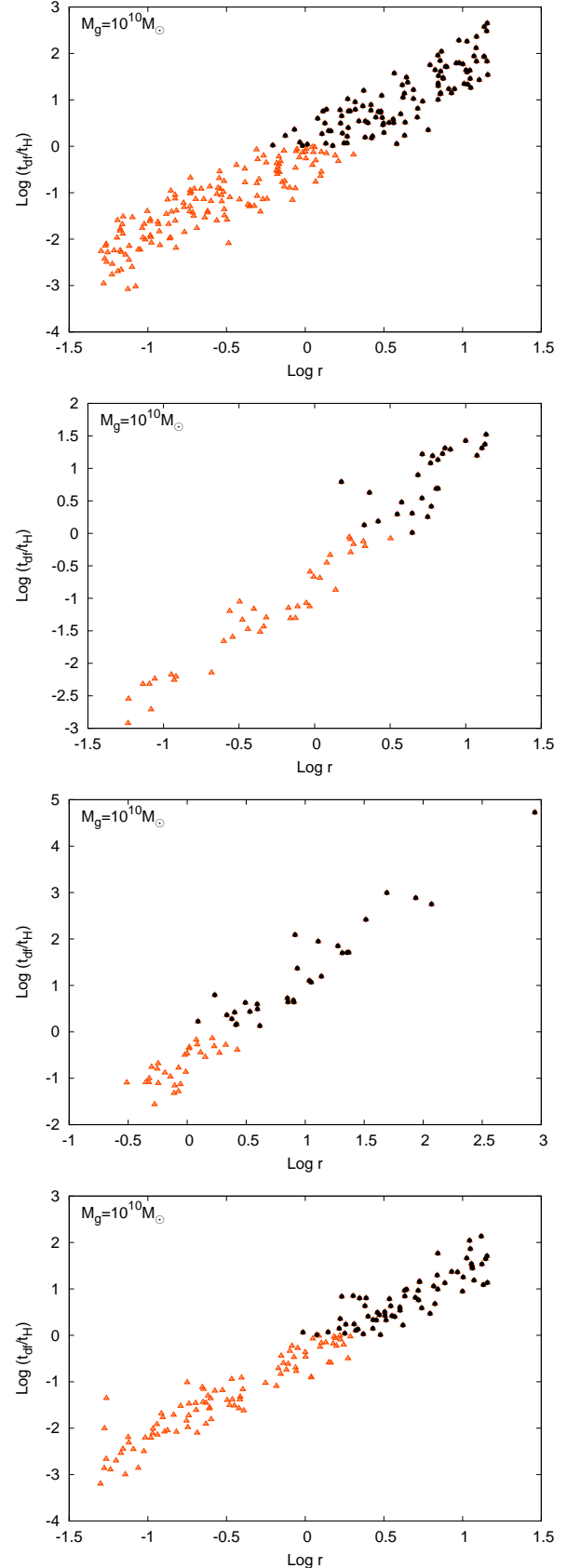


Figure 13. From top to bottom, the ratio t_{df}/t_H is shown for a sampled galaxy $M_g = 10^{10} M_\odot$ in PLS, RND, RHO and GSS models, respectively. Decayed clusters (triangles) lie all in a region whose radius is roughly $r \sim 3 \text{ kpc}$.

Table 1. $M_{\text{NSC}} - M_g$ scaling relation parameters for various models.

Model	b	ϵ_{r_b}	a	ϵ_{r_a}
s=2	0.955	0.015	-0.206	0.021
PLS	1.0682	0.0030	-0.4415	0.0037
RND	1.0482	0.0051	-0.3778	0.0062
GSS	1.0707	0.0028	-0.4391	0.0034
RHO	1.0488	0.0061	-0.6525	0.0075

Column 1: model name as explained in Section 2.2. Column 2-5: slope b and zeropoint a and relative errors.

Table 2. $M_{\text{NSC}} - M_g$ scaling relation parameters as given in literature.

Model	b	ϵ_{r_b}
LKB12	1.18	0.16
EG12	0.90	0.21
SG13	0.88	0.19

Column 1: reference paper name. Column 2-3: slope b and and relative error.

relations. At this scope, in Figure 15 and Figure 16 we report, respectively, the NSC masses as functions of the host galaxy velocity dispersion and bulge mass of our models compared with observed data. Note that due to the somewhat ill definition of the bulge, the relation M_{NSC} vs M_b is not very reliable.

4.1 $M_{\text{NSC}} - M_g$ relation

It has been shown that the NSC mass correlates better with the total galaxy mass, while the correlation with the bulge is not statistically very significant (Erwin & Gadotti 2012).

We obtained a power law best-fitting for our sampled correlation between M_{NSC} and M_g in the form

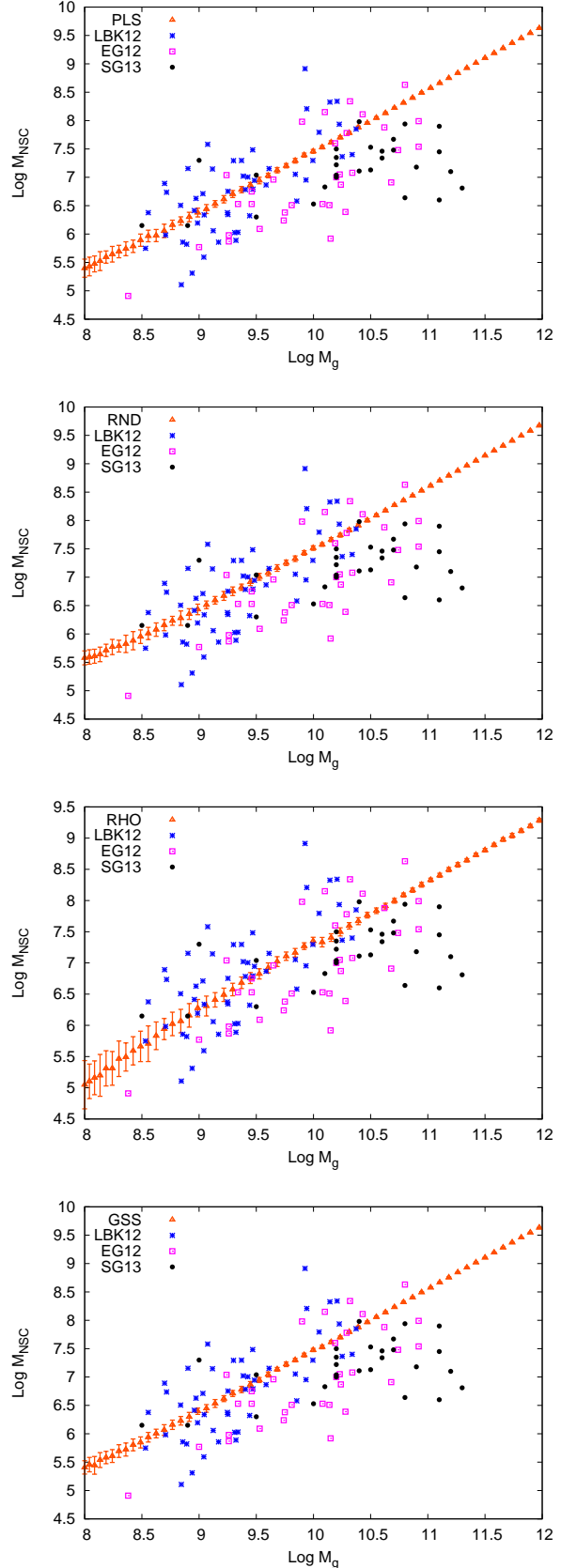
$$\text{Log} \left(\frac{M_{\text{NSC}}}{10^{7.6} M_\odot} \right) = a + b \text{Log} \left(\frac{M_g}{10^{9.7} M_\odot} \right), \quad (32)$$

where the coefficients a and b (see Table 1) are computed by using the Marquardt-Levenberg nonlinear-regression algorithm. For the sake of comparison we report Table 2 the slope b of the best-fittings to the $M_{\text{NSC}} - M_g$ relations in the EG12, LKB12 and SG13 data samples.

The comparison between values in Table 1 and 2 indicates that both the analytical ($s = 2$) model and the statistical approaches (PLS, GSS, RND and RHO models) give a slope in good agreement with the observed relation, within the errors.

4.2 $M_{\text{NSC}} - M_b$ relation

Using the estimate of the bulge masses given by Equation 18, the slopes of the logarithmic correlations between M_{NSC} and M_b for our various models are given in Table 3. They compare with the slope of the observational law of SG1 data sample, which is $b = 0.88 \pm 0.19$, in agreement, within the error bar, with all theoretical predictions.

**Figure 14.** NSC masses with respect hosts masses. Predicted values (triangles) are compared with data given in LKB12 (stars), EG12 (squares) and SG13 (filled circles).

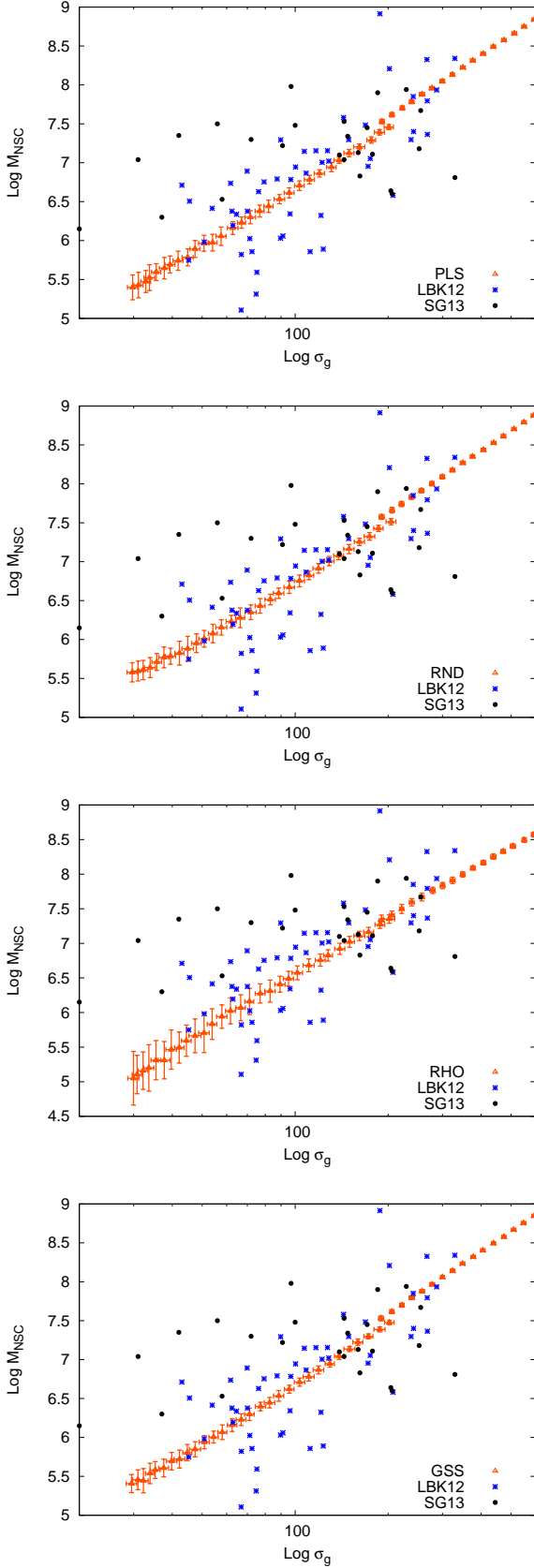


Figure 15. NSC masses vs. hosts velocity dispersion. Predicted values (triangles) are compared with data given in LKB12 (stars) and SG13 (filled circles).

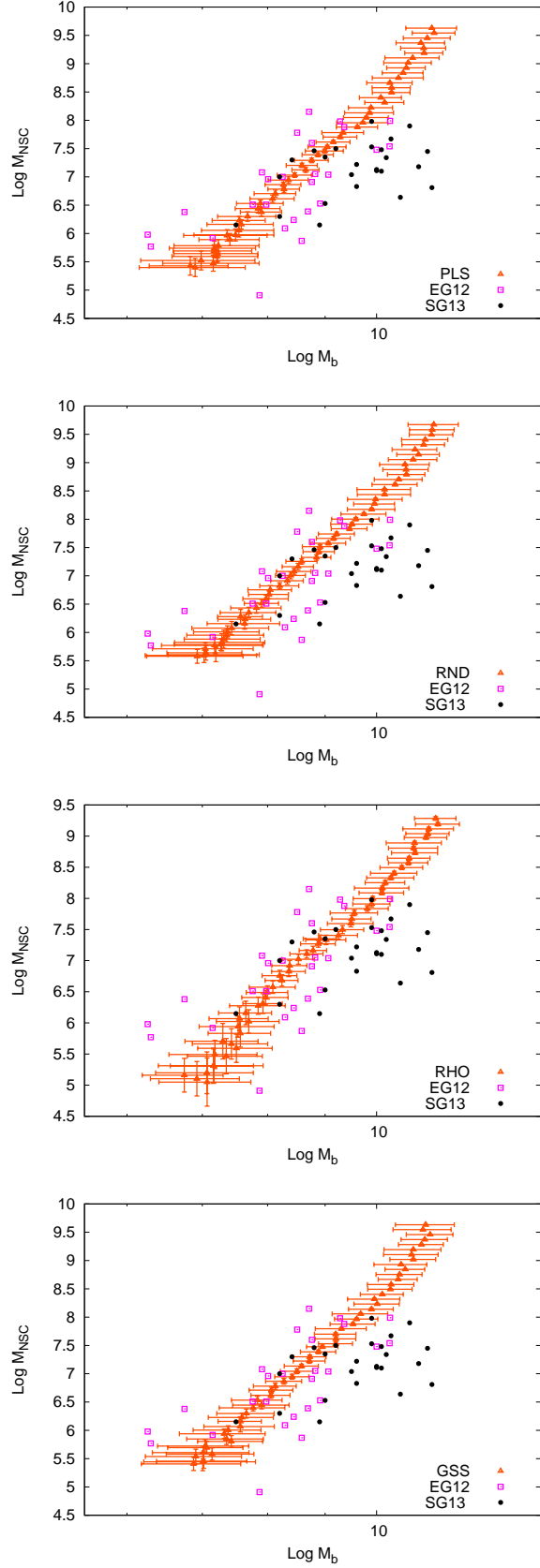


Figure 16. NSC masses with respect hosts bulge masses. Predicted values with errors (triangles) are compared with data given EG12 (squares) and SG13 (filled circles).

Table 3. $M_{\text{NSC}} - M_B$ relation parameters for various models.

Model	b	ϵ_{r_b}	a	ϵ_{r_a}
s=2	0.732	0.028	1.36	0.27
PLS	0.971	0.019	-1.37	0.20
RND	0.960	0.017	-1.22	0.19
GSS	1.000	0.028	-1.61	0.30
RHO	0.840	0.012	-0.31	0.13

Column 1: model name as explained in Section 2.2. Column 2-5: slope b and zero-point a with relative errors.

Table 4. $M_{\text{NSC}} - \sigma_g$ relations parameters for various models.

Model	b	ϵ_{r_b}	a	ϵ_{r_a}
s=2	2.410	0.036	-0.336	0.021
PLS	2.699	0.015	-0.5816	0.0072
RND	2.649	0.019	-0.5139	0.0093
GSS	2.705	0.014	-0.5781	0.0067
RHO	2.651	0.012	-0.788	0.012

Column 1: model name as explained in Section 2.2. Column 2-5: slope b and zero-point a and relative errors. The relation used is: $\log(M_{\text{NSC}}/10^{7.6}M_\odot) \propto \log(\sigma_g/200\text{km s}^{-1})$.

4.3 $M_{\text{NSC}} - \sigma_g$ relation

The correlation between the NSC mass and the host galaxy velocity dispersion is probably the most interesting correlation to analyse, because it can give useful hints about relations between the two types of CMOs (SMBHs and NSCs). If for NSCs and SMBHs a similar mass-sigma correlation holds, one could infer that they shared the same evolutionary path.

Actually, our theoretical results point towards a weak scaling of the NSC mass with σ_g . As shown in Tables 4 and 5, all our theoretical models give a slope for the mass-sigma relation $2 < b_\sigma < 3$, in good agreement with that obtained by observations and just slightly larger than that obtained with the simple dynamical friction based analytical considerations in Sect. 2.1. Given that the SMBHs mass depends more strongly on σ_g , this result would likely imply that NSCs and SMBHs do not share the same evolutionary history, or, at least, that some different kind of interaction between the two types of objects and the background occurred.

5 TIDAL DISRUPTION EFFECTS

In the previous Sections we showed that the dry-merger scenario provides scaling relations connecting the NSC masses with global parameters of their hosts. However, there are at least two effects which could prevent the formation of NSCs, acting in competition with the dynamical friction process:

Table 5. $M_{\text{NSC}} - \sigma_g$ relations parameters from the literature.

Model	b	ϵ_{r_b}
LKB12	2.73	0.29
SG13	2.11	0.31

Column 1: sample name. Column 2-3: slope b and and relative error.

the two-body relaxation mechanism and the tidal heating process. In this Section we study their effects on the formation of NSCs and show that the scaling laws derived in this case still agree with observations in the whole range of galaxy masses.

During its lifetime, a GC undergoes internal dynamical evolution experiencing two-body relaxation and suffering of external tidal perturbations that, in some cases, can lead to its total, or partial, dissolution. Actually, it is well known that two-body encounters between stars may bring some of them beyond the GC tidal boundary after few hundred times the typical two-body relaxation time (Spitzer 1987). Gieles, Lamers & Baumgardt (2008), using results by Baumgardt (2001), gave the following formula for the evaluation of the dissolution time of a cluster due to the effects of two-body encounters:

$$\tau_{\text{dis}}(\text{Gyr}) = \left(\frac{M}{10^4 M_\odot} \right)^{0.62} \left(\frac{r}{\text{kpc}} \right) \left(\frac{v_c}{220 \text{ km s}^{-1}} \right)^{-1} (1 - e), \quad (33)$$

where M is the GC mass, r is the distance from the galactic centre, v_c the circular velocity at r , and e the eccentricity of the orbit.

Moreover, gravitational encounters between the stellar system and a perturber (which could be a black hole), the disc, or the nucleus, of the galaxy, could lead to the destruction of the system over a time comparable to the dynamical friction decay time. This implies that the phenomenon of cluster destruction cannot be neglected. In the case in which the perturber is a point mass, a black hole, Spitzer (1958, 1987) studied the effect of such perturbation on a stellar system of mass M_s , in the hypothesis that the duration of the encounter is short compared to the internal crossing time of the cluster. This is the impulse approximation, which assumes that as a consequence of the encounter, stars in the perturbed system suffer only a change in their velocities, but not in the positions. Moreover, due to the slow duration of the perturbation, the cluster trajectory can be approximated with a straight line. Under this hypothesis, it is possible to show that the cluster, as a consequence of the gravitational encounter with the perturber of mass M_p , gains an energy per unit mass:

$$\Delta E = \frac{4G^2 M_p^2}{3V^2 b^4} \langle R^2 \rangle, \quad (34)$$

where V is the relative velocity between the two objects, b is the impact parameter and $\sqrt{\langle R^2 \rangle}$ is the mean dimension of the perturbed cluster.

A number of studies have been devoted to generalize this result to an extended spherical perturber with an arbitrary mass distribution (Aguilar & White 1985; Gnedin, Hernquist & Ostriker 1999; Gnedin & Ostriker 1997), and to the case where the perturber is a spherical nucleus of stars embedded in a triaxial ellipsoid (Ostriker, Binney & Saha 1989; Capuzzo-Dolcetta 1993).

Defining $U(b/r_h)$ the ratio between the impulsive energy change due to a perturber of half mass radius r_h and that caused by a point of same mass, M_p , the total change in energy per unit mass caused by a mass distribution is given by:

$$\Delta E = \frac{4G^2 M_p^2}{3V^2 b^4} \langle r^2 \rangle U(b/r_h); \quad (35)$$

where the function $U(b/r_h)$ drops rapidly to 0 when b/r_h approaches zero, while tends to 1 for large values of b/r_h and should be evaluated numerically.

If the energy change exceeds the internal gravitational energy of the system per unit mass (Spitzer 1958):

$$E = \frac{3}{5} \frac{GM_s}{R_s}, \quad (36)$$

the cluster is disrupted. The typical time over which this disruption occurs is

$$t_{\text{dis}} = \frac{E}{\Delta E} nT. \quad (37)$$

where T is the orbital period of the cluster and n is the number of encounters within a period.

Further, the encounters are characterized by two extreme regimes: the catastrophic regime, if a single encounter could disrupt completely the system, and the diffusive regime, when the cumulative effect of encounters leads to the disruption of the system over a longer time. Defining as b_M the impact parameter that corresponds to an energy enhancement equal to the internal gravitational energy of the system, i.e. $\Delta E = E$, it is possible to determine the duration of the encounter, $t_{\text{enc}} \sim b_M/\sigma_{\text{rel}}$, that is the typical time-scale which discriminates between the two regimes: hence a catastrophic collision occurs if the duration of the encounter is short compared to the crossing time of the cluster, $t_{\text{cr}} \sim R_s/V$; on the other hand, slower encounter leads to the diffusive regime.

Therefore, in the case of the catastrophic regime ($t_{\text{enc}} < t_{\text{cr}}$), the typical disruption time is given by:

$$t_{\text{cat}} \simeq \frac{k_{\text{cat}}}{G\rho_p} \left(\frac{GM_s}{R_s^3} \right)^{1/2}, \quad (38)$$

where ρ_p is the perturber density, and k_{cat} a constant. In the diffusive regime $t_{\text{enc}} \geq t_{\text{cr}}$, instead, it is possible to show that the disruption time is given by:

$$t_{\text{dif}} = \frac{0.043}{W} \frac{\sigma_{\text{rel}} M_s r_h^2}{GM_p \rho_p R^3}, \quad (39)$$

where W is defined as:

$$W = \int \frac{U(x)}{x^3} dx, \quad (40)$$

where $x = b/r_h$ and $U(x)$ is defined above, and should be computed numerically.

Tidal effects are accounted for in our calculations in the above framework, so to investigate their role on the expected value of the NSC mass. In Figure 17 we compare the dynamical friction time, t_{df} , evaluated using Equation 11, the dissolution time, t_{dis} , given in Equation 37, and the tidal disruption time in the catastrophic regime t_{cat} for three values of the galaxy mass ($M_g = 10^8, 10^{10}, 10^{12} M_\odot$) as a function of the distance, r , from the centre of the host galaxy. On the other hand, the disruption time in the diffusive regime, t_{dif} , is not reported in the graph since it is systematically greater than the other time-scales. We performed the estimation setting the GC mass to $M = 10^6 M_\odot$ and selecting a circular orbit. Looking at Figure 17, it is clear that while in small galaxies ($M < 10^{10} M_\odot$), the dynamical friction time

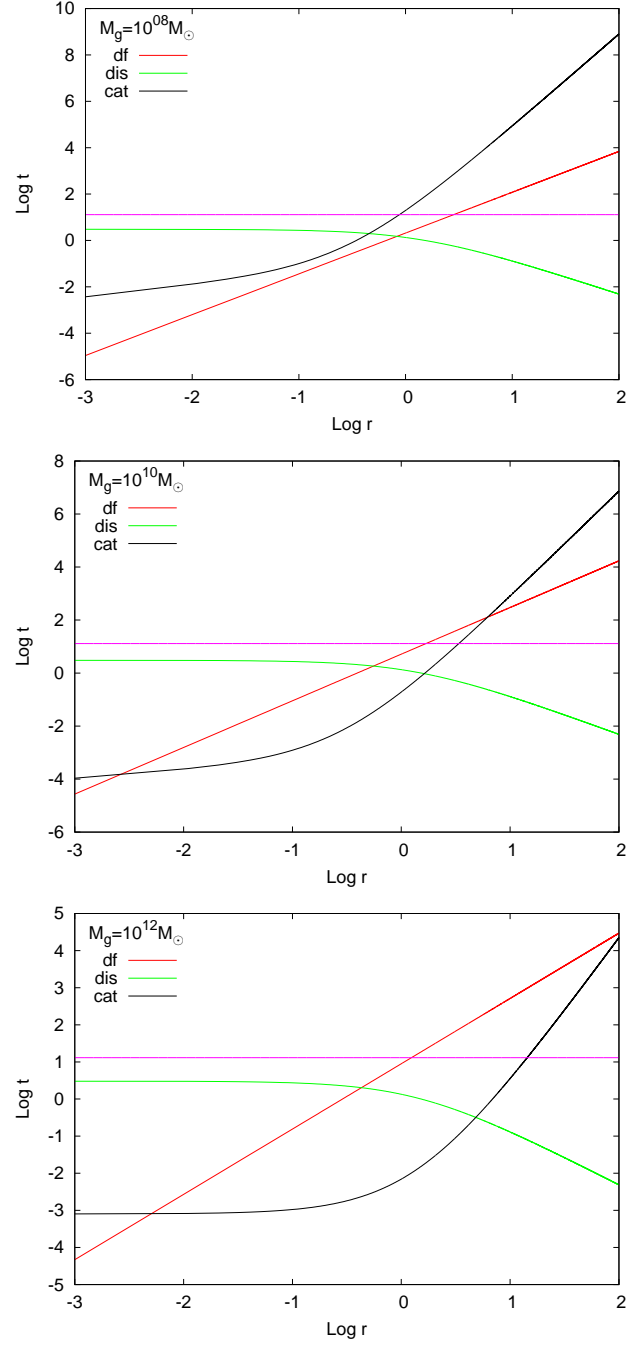


Figure 17. Dynamical decay and disruption times for a globular cluster on circular orbit for three different galaxy masses (from top to bottom: $10^8 - 10^{10} - 10^{12} M_\odot$). Times are given in units of 1-Gyr while positions are given in units of 1kpc. In smaller galaxies, friction process dominates on all length scales, while in heavier systems the tidal disruption is much more rapid in a region 1kpc around, suppressing the friction mechanism.

is smaller than the disruption times over all length scales, in more massive galaxies it dominates only in a region around the centre of the galaxy, while in the range 0.1 – 100kpc dominates the tidal effect due to the interaction between the cluster and the galactic nucleus, suppressing the role of dynamical friction process and, then, the consequent formation of a NSC.

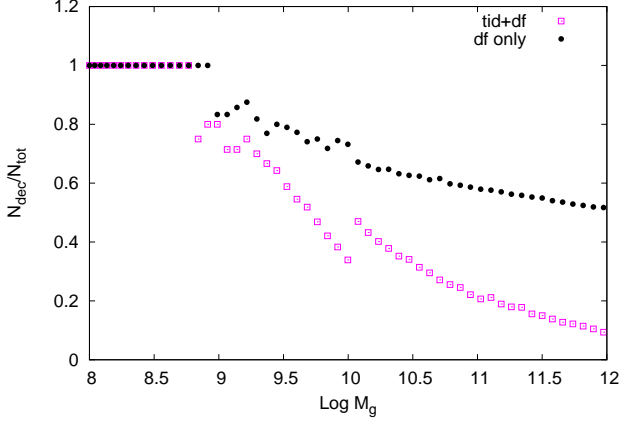


Figure 18. The fraction of the number of decayed clusters to their total number considering only df (filled circles) or taking into account the tidal shock mechanism (empty squares) in the RND model. As you can see, the number of decayed clusters in massive galaxies decrease by a factor 5 when tidal disruption is considered, changing by roughly the same factor the NSC final mass.

The two competitive processes, make that the number of decayed clusters depends strongly on their space distribution.

In the RND, PLS and GSS models, we set $d = 50\text{pc}$ as minimum distance from the galaxy centre of the GC sample. Clusters lying in the central $50 - 100\text{pc}$, which are massive enough ($M \gtrsim 10^6 M_\odot$) or on eccentric orbits are likely to decay and give a large contribute to the final NSC mass. Figure 18 shows the fraction of the number of decayed clusters to the total number for the RND model, considering or not the tidal effect.

While in small galaxies almost all the clusters have time to decay, even if the tidal disruption mechanism is active, in massive galaxies the perturbations induced by the external field corresponds to a reduction of the NSC mass.

However, the action of the tidal disruption mechanism does not change dramatically the final mass of the NSC; in fact, the decrease in mass of the final nuclear cluster is reduced of only the 20% respect to the case when the tidal action of the galaxy on the clusters is not considered. Hence, the effect of tidal processes in such models is not too important in the determination of the final NSC masses. On the other hand, since in the RHO model the minimum distance from the galaxy centre allowed for GC formation is given by the constraint that the GCS mass profile follows a Dehnen profile, it could exceed $\sim 50\text{pc}$. This implies that many clusters lie in the region in which the tidal effects dominate, affecting strongly the final mass of the NSC. In this case, as we can see in Figure 19, the number of decayed clusters in very massive galaxies drops to zero avoiding the formation of NSCs.

The difference between the RHO model and the others, where the GCs positions are sampled randomly, puts in evidence two interesting things: the mass distribution of the clusters is not very important in deriving the NSC mass, but instead, what care is how clusters are distributed within the galaxy. This because at intermediate radial scales the disruption time is smaller than the decay time, while it is longer

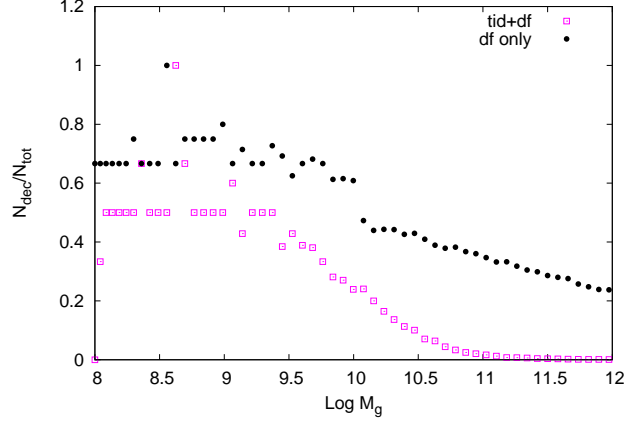


Figure 19. Same as in Figure 18, but for the RHO model. In this case, the number of decayed clusters for massive galaxies drops to 0 and there is no NSC formation.

in the central region. Hence, a concentrated spatial distribution allows the formation of the NSC because clusters in the innermost region of the galaxy decay rapidly.

In Figure 20 we report the values of NSC masses with respect to host masses for all the models considered taking into account the tidal disruption process. It is seen that in the case of the RHO model the tidal interaction (tidal heating) inhibits the NSC formation for galaxies masses above $3 - 4 \times 10^{10} M_\odot$, putting in evidence how important the spatial distribution of the clusters is. It is interesting noting that in this case, the scaling relations found are again in good agreement with the observations, if we restrict the comparison to the actually observed range of masses ($10^8 - 10^{11} M_\odot$).

6 SUMMARY AND CONCLUSIONS

We found that the dry-merger scenario predicts masses for NSCs and scaling laws between them and their host galaxies in excellent agreement with observations.

The summary of our work is:

- (i) an analytical treatment to estimate the formation and growth of NSCs masses has been developed;
- (ii) reliable galaxy models have been provided, as it has been shown comparing theoretical and observational global properties;
- (iii) assuming a power-law mass function and a uniform spatial distribution, the analytical predictions fit very well observations;
- (iv) the consequences of different initial mass distributions of the set of GCs in the host galaxies on the NSC final mass have been investigated from a statistical point of view, by sampling, for each galaxy, its GCS and considering how many clusters were able to sink to the galactic centre within a Hubble time;
- (v) by means of the statistical approach, we obtained some useful parameters, such as the GC mean mass and the number of survived clusters, which result in good agreement with observations;
- (vi) scaling laws which connect the NSC parameters with total mass, velocity dispersion and bulge mass of the host,

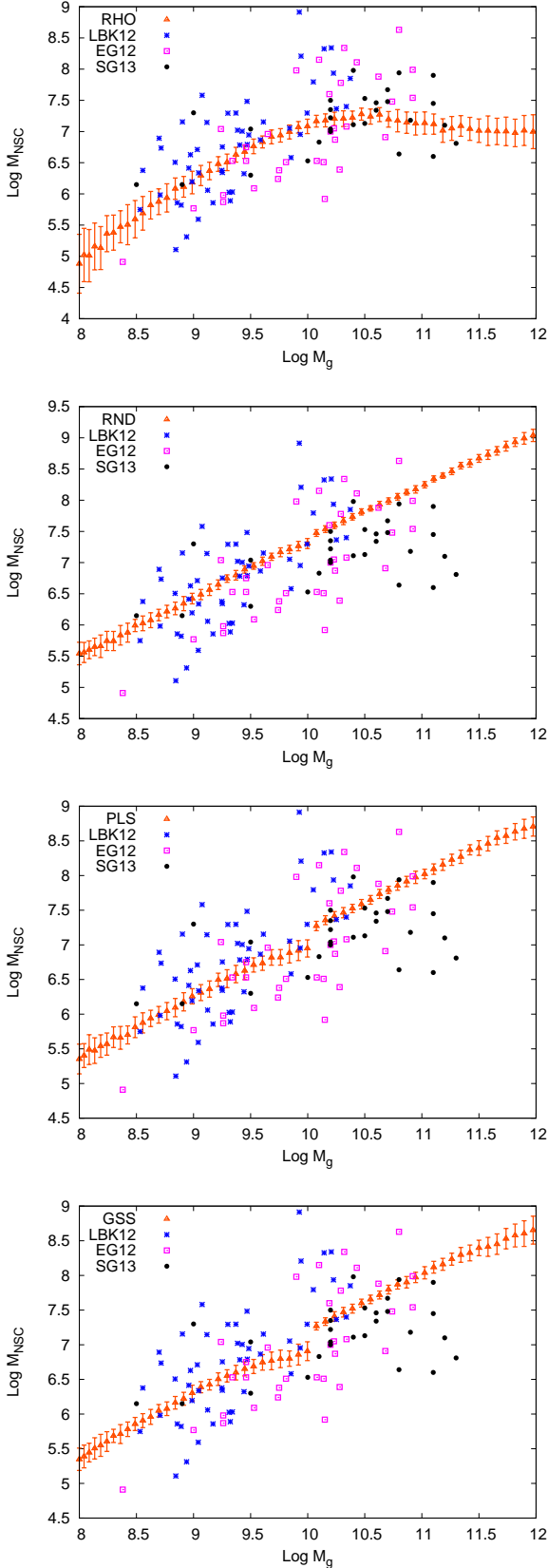


Figure 20. NSC masses as a function of the galaxy mass for all the models considered taking into account the tidal disruption processes. In each panel, triangles refer to the results of each model (as indicated in the legend) while stars, squares and filled circles refer to observations.

have been deduced; the agreement found between all the models considered and observations indicates that the GC mass distribution does not play a crucial role in determining the final NSC mass;

(vii) the role of tidal disruption mechanism has been investigated under different assumptions for the spatial and mass distributions of GCs in their host galaxies: in RND, PLS and GSS models the tidal heating causes a decrease of predicted NSC masses from few percent in small galaxies (down to $10^{10} M_\odot$) to 20% in heavier galaxies. On the other hand, tidal disruption strongly affects NSC formation in the RHO model, where the predicted NSC masses are almost constant in the range $10^{10} - 10^{11} M_\odot$. An important result is that the best comparison for the NSC mass versus galactic host mass correlation is obtained when GCs have an initial spatial distribution equal to that of the galaxy, assumed to be in the Dehnen's form. This because the relation shows the same flattening at high galactic mass than observed, while in the case of flat initial density profile for GCs, the $M_{\text{NSC}} - M_g$ relation keeps raising at high masses.

The overall conclusion is that the migratory-merger model for the formation of dense stellar agglomerates in galactic centers seems to be valid for a large range of types and masses of galaxies.

APPENDIX A

Considering as density law the γ profile in Equation 27 leads to:

$$N(r) = N \left(\frac{r}{r + R_g} \right)^{3-\gamma}, \quad (41)$$

and the NSC mass is thus given by:

$$M_{\text{NSC}}(t) = \Gamma \int_{M_l}^{M_u} M^{1-s} \left(\frac{CM^{0.38}}{CM^{0.38} + R_g} \right)^{3-\gamma} dM, \quad (42)$$

being $C = C(M_g, R_g, \gamma, e; t)$ as in Equation 30.

The explicit expression in this case is given by:

$$M_{\text{NSC}} = \frac{\mathcal{F} [-M_{u2}^k F_1(a, b; c; z(M_u)) + M_{l2}^k F_1(a, b; c; z(M_l))]}{R_g^{3-\gamma} (0.67(\gamma - 3) + 1.76(s - 2))}, \quad (43)$$

with $\mathcal{F} = 1.76\Gamma_0 C^{3-\gamma}/\rho_0$, $k = 0.38(3 - \gamma) + 2 - s$ and ${}_2F_1(a, b; c; z)$ the Gauss' Hypergeometric Function, defined as:

$${}_2F_1(a, b; c; z) = \frac{\Gamma(c)}{\Gamma(b)\Gamma(b-c)} \int_0^1 \frac{t^{b-1}(1-t)^{c-b-1}}{(1-tz)^a} dt, \quad (44)$$

where $\Gamma(x)$ is the classic Euler's Gamma function (Abramowitz & Stegun 1964)

and the arguments in Equation 43 are:

$$\begin{aligned} a &= 3 - \gamma, \\ b &= -\frac{0.67(\gamma - 3) + 1.76(s - 2)}{0.67}, \\ c &= -\frac{0.67(\gamma - 4) + 1.76(s - 2)}{0.67}, \\ z &= -\frac{CM^{0.38}}{R_g}. \end{aligned}$$

REFERENCES

- Abramowitz M., Stegun I. A., 1964, *Handbook of Mathematical Functions with Formulas, Graphs, and Mathematical Tables*. Dover Publications, New York
- Aguilar L. A., White S. D. M., 1985, *ApJ*, 295, 374
- Antonini F., 2013a, *ApJ*, 763, 62
- Antonini F., 2013b, *ApJ*, 763, 62
- Antonini F., Capuzzo-Dolcetta R., Mastrobuono-Battisti A., Merritt D., 2012, *ApJ*, 750, 111
- Arca-Sedda M., Capuzzo-Dolcetta R., 2014, *ApJ*, 785, 51
- Ashman K. M., Zepf S. E., 1998, *Globular Cluster Systems*. Cambridge University Press, New York
- Baumgardt H., 1998, *A & A*, 330, 480
- Baumgardt H., 2001, *MNRAS*, 325, 1323
- Bekki K., 2010, *MNRAS*, 401, 2753
- Bekki K., Couch W. J., Shioya Y., 2006, *ApJL*, 642, L133
- Bekki K., Graham A. W., 2010, *ApJL*, 714, L313
- Böker T., 2010, in de Grijs R., Lépine J. R. D., eds, *IAU Symposium Vol. 266 of IAU Symposium, Nuclear star clusters*. Cambridge University Press, pp 58–63
- Böker T., 2012, preprint arxiv:1210.5368
- Böker T., Laine S., van der Marel R. P., Sarzi M., Rix H.-W., Ho L. C., Shields J. C., 2002, *AJ*, 123, 1389
- Cappellari M., Bacon R., Bureau M., Damen M. C., Davies R. L., de Zeeuw P. T., Emsellem E., Falcón-Barroso J., Krajnović D., Kuntschner H., McDermid R. M., Peletier R. F., Sarzi M., van den Bosch R. C. E., van de Ven G., 2006, *MNRAS*, 366, 1126
- Capuzzo-Dolcetta R., 1993, *ApJ*, 415, 616
- Capuzzo-Dolcetta R., Miocchi P., 2008a, *ApJ*, 681, 1136
- Capuzzo-Dolcetta R., Miocchi P., 2008b, *MNRAS*, 388, L69
- Capuzzo-Dolcetta R., Vicari A., 2005, *MNRAS*, 356, 899
- Côté P., Blakeslee J. P., Ferrarese L., Jordán A., Mei S., Merritt D., Milosavljević M., Peng E. W., Tonry J. L., West M. J., 2004, *ApJS*, 153, 223
- Côté P., Piatek S., Ferrarese L., Jordán A., Merritt D., Peng E. W., Hasegan M., Blakeslee J. P., Mei S., West M. J., Milosavljević M., Tonry J. L., 2006, *ApJS*, 165, 57
- Dehnen W., 1993, *MNRAS*, 265, 250
- Dullo B. T., Graham A. W., 2012, *ApJ*, 755, 163
- Erwin P., Gadotti D. A., 2012, *Advances in Astronomy*, 2012
- Ferrarese L., Côté P., Dalla Bontà E., Peng E. W., Merritt D., Jordán A., Blakeslee J. P., Hasegan M., Mei S., Piatek S., Tonry J. L., West M. J., 2006, *ApJL*, 644, L21
- Gieles M., Lamers H. J. G. L. M., Baumgardt H., 2008, in Vesperini E., Giersz M., Sills A., eds, *IAU Symposium Vol. 246 of IAU Symposium, Star Cluster Life-times: Dependence on Mass, Radius and Environment*. pp 171–175
- Gnedin O. Y., Hernquist L., Ostriker J. P., 1999, *ApJ*, 514, 109
- Gnedin O. Y., Ostriker J. P., 1997, *ApJ*, 474, 223
- Gnedin O. Y., Ostriker J. P., Tremaine S., 2014, *ApJ*, 785, 71
- Graham A. W., 2004, *ApJL*, 613, L33
- Graham A. W., 2012, *MNRAS*, 422, 1586
- Häring N., Rix H.-W., 2004, *ApJL*, 604, L89
- Harris G. L. H., Poole G. B., Harris W. E., 2014, *MNRAS*, 438, 2117
- Hartmann M., Debattista V. P., Seth A., Cappellari M., Quinn T. R., 2011, *MNRAS*, 418, 2697
- Just A., Khan F. M., Berczik P., Ernst A., Spurzem R., 2011, *MNRAS*, 411, 653
- King A., 2003, *ApJL*, 596, L27
- King A., 2005, *ApJL*, 635, L121
- Lauer T., et al. 2007, *ApJ*, 664, 226
- Leigh N., Böker T., Knigge C., 2012, *MNRAS*, 424, 2130
- Marconi A., Hunt L. K., 2003, *ApJL*, 589, L21
- Mastrobuono-Battisti A., Perets H. B., 2013, *ApJ*, 779, 85
- McLaughlin D. E., Harris W. E., Hanes D. A., 1994, *ApJ*, 422, 486
- McLaughlin D. E., King A. R., Nayakshin S., 2006, *ApJL*, 650, L37
- Merritt D., 2006, *Rep. Prog. Phys.*, p. 2513
- Milosavljević M., 2004, *ApJL*, 605, L13
- Nayakshin S., Wilkinson M. I., King A., 2009, *MNRAS*, 398, L54
- Neumayer N., 2012, preprint arxiv:1211.1795
- Neumayer N., Walcher C. J., 2012, *Advances in Astronomy*, 2012
- Ostriker J. P., Binney J., Saha P., 1989, *MNRAS*, 241, 849
- Perets H. B., Mastrobuono-Battisti A., 2014, *ApJL*, 784, L44
- Pesce E., Capuzzo-Dolcetta R., Vietri M., 1992, *MNRAS*, 254, 466
- Rossa J., van der Marel R. P., Böker T., Gerssen J., Ho L. C., Rix H.-W., Shields J. C., Walcher C.-J., 2006, *AJ*, 132, 1074
- Scott N., Graham A. W., 2013, *ApJ*, 763, 76
- Seth A., Cappellari M., Neumayer N., Caldwell N., Bastian N., Olsen K., Blum R., Debattista V. P., McDermid R., Puzia T., Stephens A., 2010, in Debattista V. P., Popescu C. C., eds, *American Institute of Physics Conference Series Vol. 1240 of American Institute of Physics Conference Series, Nuclear Star Clusters and Black Holes*. pp 227–230
- Silk J., Rees M. J., 1998, *A & A*, 331, L1
- Spitzer L., 1987, *Dynamical evolution of globular clusters*. Princeton University Press, Princeton
- Spitzer Jr. L., 1958, *ApJ*, 127, 17
- Tremaine S. D., Ostriker J. P., Spitzer Jr. L., 1975, *ApJ*, 196, 407
- Turner M. L., Côté P., Ferrarese L., Jordán A., Blakeslee J. P., Mei S., Peng E. W., West M. J., 2012, *ApJS*, 203, 5
- van den Bosch R. C. E., Gebhardt K., Gültekin K., van de Ven G., van der Wel A., Walsh J. L., 2012, *Nature*, 491, 729
- Whitmore B. C., Chandar R., Schweizer F., Rothberg B., Leitherer C., Rieke M., Rieke G., Blair W. P., Mengel S., Alonso-Herrero A., 2010, *AJ*, 140, 75